Focussed on the Failure Analysis of Materials and Structures

Visual Abstract

Acoustic analysis using symmetrised implicit midpoint rule

N. Razali, N.B. Masnoor, S. Abdullah, M.F.H.M. Zainaphi
Universiti Kebangsaan Malaysia, Malaysia
helyna@ukm.edu.my, https://orcid.org/0000-0001-9333-3012
nisabalqismasnoor@gmail.com, shahrum@ukm.edu.my, faizhilmi9797@gmail.com

ABSTRACT. In wave propagation phenomena, time-advancing numerical methods must accurately represent the amplitude and phase of the propagating waves. The acoustic waves are non-dispersive and non-dissipative. However, the standard schemes both retain dissipation and dispersion errors. Thus, this paper aims to analyse the dissipation, dispersion, accuracy, and stability of the Runge–Kutta method and derive a new scheme and algorithm that preserves the symmetry property. The symmetrised method is introduced in the time-of-finite-difference method for solving problems in aeroacoustics. More efficient programming for solving acoustic problems in time and space, i.e. the IMR method for solving acoustic problems, an advection equation, compares the square-wave and step-wave Lax methods with symmetrised IMR (one-and two-step active). The results of conventional methods are usually unstable for hyperbolic problems. The forward time central space square equation is an unstable method with minimal usefulness, which can only study waves for short fractions of one oscillation period. Therefore, nonlinear instability and shock formation are controlled by numerical viscosities such as those discussed with the Lax method equation. The one- and two-step active symmetrised IMR methods are more efficient than the wave method.

KEYWORDS. Numerical method; Runge–Kutta method; IMR; Symmetrisation.

OPEN ACCESS

Citation: Razali, N., Masnoor, N.B., Abdullah, S., Zainaphi, M.F.H.M., Acoustic analysis using symmetrised implicit midpoint rule, Frattura ed Integrità Strutturale, 61 (2022) 214-229.

Received: 14.02.2022
Accepted: 30.04.2022
Online first: 24.05.2022
Published: 01.07.2022

INTRODUCTION

Acoustic problems are governed by equations of compressible flows, namely, Euler equations or Navier–Stokes equations. In wave propagation theory, the propagation characteristic is encoded in the dispersion relationships of the governing equation. Numerical schemes that minimise these errors are required because acoustic waves are nondispersive and nondissipative. The pollution effect resulting from dispersion is a well-known, thoroughly researched phenomenon of the finite-element method, particularly for the acoustic problem [12, 1, 10]. The concern is that a local mesh refinement is unable to adjust for the numerical error, which is obtained and gathered in other parts of the model.

Previous research found that with the boundary element method, a pollution effect due to dispersion is rare. Additionally, numerical damping in the boundary element method can account for a pollution effect [13]. A deeper look into numerical damping indicated this has equivalent effects on the phase error of the finite-element method [14, 15].

Pollution effect happens when a local mesh refinement is unable to adapt for the numerical error, which is created and accumulated in other parts of the model. Numerical damping in the boundary element method can also account for a pollution effect. Conventional numerical methods such as the explicit Runge–Kutta (RK) methods maintain dissipation and dispersion errors. To clarify wave propagation, numerical solutions have to be time accurate. A symmetric RK method has asymptotic error expansion in even powers of step size. When used with the extrapolation technique, the order subsequently grows two at a time, hence boosting the accuracy of the method [17, 3]. However, when these methods are used to solve stiff cases, other problems, such as oscillations in the numerical solutions, might occur as a result of the stability function, which changes when the problem is stiff. Order reduction effects might also occur in cases where the order of the method is governed by the stage order. Hence, a modified symmetry RK method is essential to eliminate the constraints and simultaneously preserve the symmetry property of the numerical method.

Research has been conducted to obtain a modified algorithm in either the finite-element [18] method or the boundary-element method [1]. Several researchers use RK methods with low dissipation and low dispersion, using explicit RK schemes with various orders [8, 11]. However, explicit methods are not appropriate for dealing with stiff cases. When several components of a solution decay more quickly than others, stiffness occurs. The actual solution to these problems is extremely stable, whereas the numerical solutions are quite unstable. To keep the numerical approximations constrained, a step size less than the accuracy is required. The increased computation may result in an unacceptably large roundoff error. This step size restriction is common of explicit methods, in which the step size is limited by stability rather than accuracy. Implicit methods are highly stable, and study into the dissipation and dispersion of RK methods has shifted towards implicit methods with semi-implicit and diagonally implicit properties [7, 9, 16]. Many researchers have been enthusiastically developing accurate acoustic solvers by modifying either the finite-element method or the boundary-element method. Certain researchers integrate local and global methods and show their application in scattering problems with several separated finite inhomogeneous regions. They have also proven that the setup has an integrated approach for an automobile vibro-acoustic analysis, which is practical for assessing, visualising and comparing vibro-acoustic performance with predetermined design objectives, as well as recognising and quantifying the forces and sound sources in charge for the present behaviour [6]. However, these integrations pay much less attention to pollution and other related dispersion effects.

Noise generation and propagation are studied in aeroacoustics, a field of acoustic science. This approach can be used to predict sound generated by the airframe and cavities, as well as broadband noise generated by turbomachinery, in the aerodynamics and aircraft industries. In noise reduction, accurate noise prediction, which is based on a thorough understanding of the underlying physics, is necessary [2]. These mechanisms are being investigated using computational and experimental methods. On the one hand, atmospheric variability, safety, cost and reflection in wind tunnels are all issues that experimental studies face. On the other hand, advances in computing power and numerical models promise precise forecasts at a low cost. As a result, a latest area has emerged: computational aeroacoustics (CAA). CAA is an area of aeroacoustics that uses high-order numerical approaches to predict unsteady flow development and noise generation over complex geometries. To simulate aerodynamic noise generation and propagation, the full time-dependent, compressible Navier–Stokes equations are numerically resolved in CAA. Unlike conventional CFD, any issue that CAA attempts to resolve is time dependent practically by definition. As a result, flow variables with nonlinear waves over a large frequency range are produced. The highest frequency waves, which have incredibly small wavelengths, provide a severe challenge for accurate numerical simulation. Furthermore, acoustic waves have a substantially smaller amplitude than flow, necessitating the use of high-order numerical methods. Flow disturbances dissipate quickly away from a body or their source of origin in basic CFD situations. As a result, they have such a small influence on the computational domain's boundary. Acoustic waves, on the other side, decay slightly and can contaminate the solution by reflecting the computational domain at the boundary. As a result, at the artificial exterior boundaries, radiation and outflow boundary conditions must be enforced to allow the waves to escape smoothly. As a result, in recent years, new CAA numerical approaches were developed [4].

High-accuracy numerical approaches in time and space are required to model the linear and nonlinear propagation of disturbances precisely to meet the severe standards of CAA. By definition, wave propagation across a medium is linear; nonetheless, nonlinear effects occur in many real-world flows of relevance, such as sonic booms, air turbulence and internal thermo acoustic cooling processes. Efficient numerical techniques are lacking. The conventional numerical methods include Lax method determinants of accuracy and stability. The aim of this research is to construct an efficient numerical method for solving acoustic problems in time and space, and to analyse the accuracy, and stability of the new method.

METHODOLOGY

In this chapter, the studied solution can be taken further by showing the steps of the research method and selecting a problem from the Workshop Benchmark Problems in Computational Aeroacoustics (Tam 1995). Then, the derivation of the rules is shown, and the initial value problem of flux-conservative in the advection equation and the methods used to solve are analysed. The first method is the forward time central space (FTCS) square-wave method, and the second method is the step-wave Lax method. The algorithm is derived based on an analysis of the dissipation and dispersion of the RK method. The error function is determined, and the amplification (dissipation) and phase (dispersion) errors are minimised. The algorithm is also constructed such that it satisfies the algebraic characterisation of a symmetric RK and has as an order that is as high as possible. The coding for each method is established in the MATLAB program and is checked for errors. After the verification step, the selected benchmark problem is inserted into the program for computation. The computation steps are repeated for each studied method.

An s-stage RK method $R=(A,b,c)$ with step size h for the step $\left(x_{n-1,}y_{n-1}\right)\mapsto\left(x_{n,}y_{n}\right)$ is a one-step method defined by

$$\begin{aligned} Y_i &= y_{n-1}+h\sum_{j=1}^{n} a_{ij}f\left(x_{n-1}+c_jh,Y_j\right), \qquad i=1,\dots,s, \\ y_n &= y_{n-1}+h\sum_{i=1}^{s} b_i f\left(x_{n-1}+c_ih,Y_i\right), \end{aligned} \tag{1}$$

where A is an RK matrix, and b and c are vectors of weights and abscissas, respectively. The Butcher tableau for the method is given by

$$\begin{array}{c|cccc} c_1 & a_{11} & a_{12} & \cdots & a_{1s} \\ c_2 & a_{21} & a_{22} & \cdots & a_{2s} \\ \vdots & \vdots & \vdots & \ddots & \vdots \\ c_s & a_{s1} & a_{s2} & \cdots & a_{ss} \\ \hline & b_1 & b_2 & \cdots & b_s \end{array} \qquad \text{or} \qquad \begin{array}{c|c} c & A \\ \hline & b^T \end{array}.$$

Method R is symmetric if $-R^{-1}=R$ where $-R^{-1}$ is the adjoint of R. The algebraic characterisation of the symmetric method is then given by

$$PA+AP=eb^T, \qquad Pb=b, \qquad Pc=e-c. \tag{2}$$

where e is the $s\times 1$ vector of units, and P is the $s\times s$ permutation matrix that reverses the order of the stages with (i,j)-th element given by the Kronecker, $\delta_{i,s+1-j}$. These conditions assume that $b^Te=1$ and $Ae=c$ hold.

The stability function of an RK method is defined by

$$R(z)=1+zb^T\left(I-zA\right)^{-1}e. \tag{3}$$

If it is bounded by 1 in the left half-plane, then the method is said to be A-stable, that is when $\left|R(z)\right|\le 1$ for $z\in\mathbb{C}$ with $\operatorname{Re}(z)\le 0$.

The Implicit Midpoint Rule (IMR) is a second-order method, and the Butcher tableau is given by

$$\begin{array}{c|c} \frac{1}{2} & \frac{1}{2} \\ \hline & 1 \end{array} \tag{4}$$

The stability function for this method is given by

$$R(z)=\frac{1+\frac{z}{2}}{1-\frac{z}{2}} \tag{5}$$

Smoothing for one-step IMR is given follows:

$$\begin{array}{c|cc} \frac{1}{2} & \frac{1}{2} & 0 \\ \frac{3}{2} & 1 & \frac{1}{2} \\ \hline & \frac{3}{4} & \frac{1}{4} \end{array} \tag{6}$$

These methods are called symmetrisers, are first order and have a stability function given by

$$R(z)=\frac{1}{\left(1-\frac{z}{2}\right)^2} \tag{7}$$

The two-step symmetriser is constructed with a composition of four symmetric steps:

$$\left(\tilde{A},\tilde{b},\tilde{c}\right)=\left(\begin{bmatrix} A & 0 & 0 & 0 \\ eb^T & A & 0 & 0 \\ eb^T & eb^T & A & 0 \\ eb^T & eb^T & eb^T & A \end{bmatrix},\begin{bmatrix} b-Pv \\ b-Pu \\ u \\ v \end{bmatrix},\begin{bmatrix} c \\ e+c \\ 2e+c \\ 3e+c \end{bmatrix}\right) \tag{8}$$

This method satisfies $B(2)$ and $C(1)$, which is

$$\begin{aligned} &\tilde{b}^T\tilde{e}=2, \\ &\tilde{b}^T\tilde{c}=2+2u^Tc+2v^T\left(e+c\right), \\ &\tilde{b}^T\tilde{c}^2=2\left(1+b^Tc\right)+8u^Tc+8v^T\left(e+c\right), \\ &\tilde{b}^T\tilde{A}\tilde{c}=1+2b^Tc+4u^Tc+4v^T\left(e+c\right). \end{aligned} \tag{9}$$

where $\tilde{A}$, $\tilde{b}$ and $\tilde{c}$ are given in (8). The stability for this two-step symmetriser is given by

$$\tilde{R}(z)=1+z\tilde{b}^T\left(\tilde{I}-z\tilde{A}\right)^{-1}\tilde{e}. \tag{10}$$

Using the second-order condition in (9) and satisfying damping, i.e. the stability condition in (10), the two-step IMR with Butcher tableau is obtained as

$$\begin{array}{c|cccc} \frac{1}{2} & \frac{1}{2} & & & \\ \frac{3}{2} & 1 & \frac{1}{2} & & \\ \frac{5}{2} & 1 & 1 & \frac{1}{2} & \\ \frac{7}{2} & 1 & 1 & 1 & \frac{1}{2} \\ \hline & \frac{17}{16} & \frac{13}{16} & \frac{3}{16} & -\frac{1}{16} \end{array} \tag{11}$$

The update for two-step IMR is given by

$$u_n = \frac{-u_{n-2} + 4u_{n-1} + 10u_n + 4u_{n+1} + u_{n+2}}{16} \tag{12}$$

The stability function for two-step IMR is

$$\tilde{R}(z) = \frac{1 - \frac{z^2}{2}}{\left(1 - \frac{z}{2}\right)^4} \tag{13}$$

The two other methods, which are used as a comparison for the symmetriser, are the FTCS square-wave method

$$u_j^{n+1} = u_j^n - \frac{c\Delta t}{\Delta x}\left(u_{j+1}^n - u_{j-1}^n\right) \tag{14}$$

and the step-wave Lax method

$$u_j^n \to \frac{1}{2}\left(u_{j+1}^n + u_{j-1}^n\right) \tag{15}$$

$$u_j^{n+1} = \frac{1}{2}\left(u_{j+1}^n + u_{j-1}^n\right) - \frac{c\Delta t}{2\Delta x}\left(u_{j+1}^n - u_{j-1}^n\right) \tag{16}$$

Results and Discussion

The method is tested on the advection equation

$$\frac{\partial u}{\partial t} + C\frac{\partial u}{\partial x} = 0, \tag{17}$$

where

$$\Delta x = 1, \quad C = 1$$

and the initial condition

$$u(x,0) = u_0(x) = \begin{cases} 1 & x \le 0, x \ge 2 \\ 0 & 0 < x < 1 \\ x - 1 & 1 \le x < 2 \end{cases} \tag{18}$$

Results for advection equation: results of FTCS differencing (square-wave) method

1) CFL=0.01

Fig. 1 shows the application of the FTCS differencing (square-wave) method to the problem with CFL=0.01, and no convergence of the exact solution at any time is observed. Fig. 2 shows the results more clearly, in 3D, and with no convergence, but the exact solution is not reached. In the next step, the results are displayed by changing the CFL value and showing whether it attains convergence or reaches the exact solution.

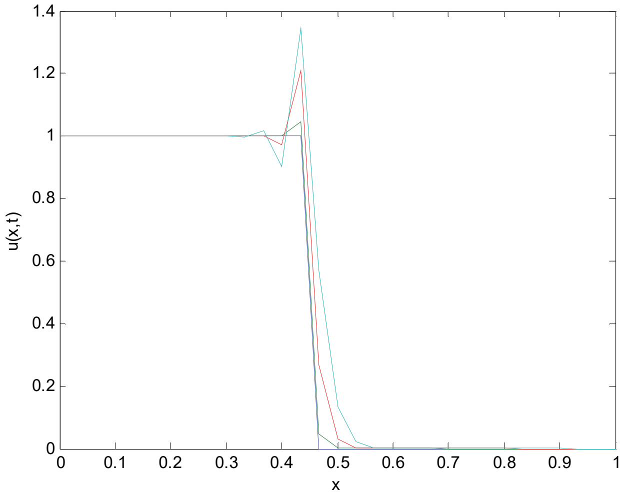

Figure 1: Square-wave (FTCS) method results for CFL=0.01

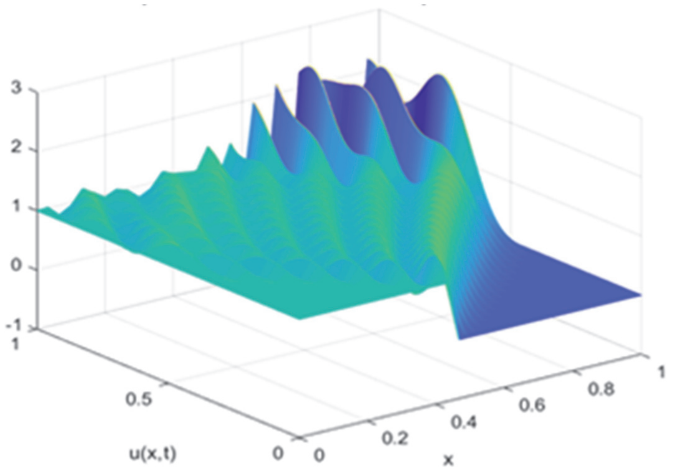

Figure 2: Square-wave (FTCS) method mesh results for CFL=0.01

2) CFL=0.5 Fig. 3 shows the application of the FTCS differencing (square-wave) method to the problem with CFL=0.5, and no convergence of the exact solution at any time is observed. These results demonstrate that instability occurred in this scenario. Fig. 4 depicts the 3D results of the applications.

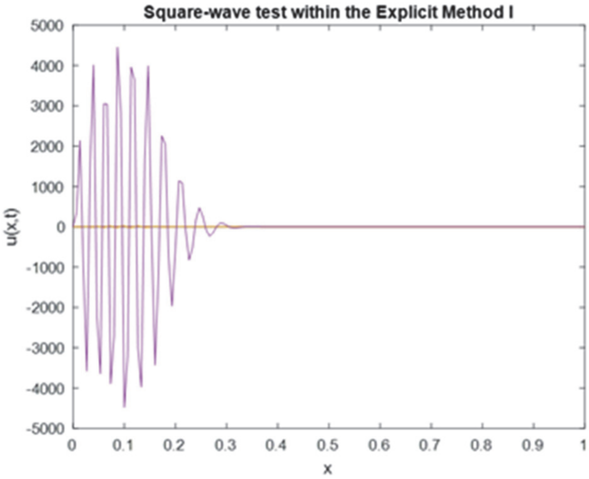

Figure 3: Square-wave (FTCS) method results for CFL=0.5

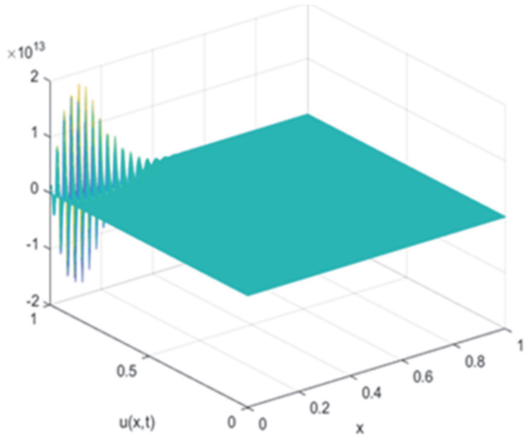

Figure 4: Square-wave (FTCS) method mesh results for CFL=0.5

3) CFL=1.0

Fig. 5 shows the application of the FTCS differencing (square-wave) method to the first problem with CFL=1.0, and no convergence of the exact solution at any time is noted. These results show that instability occurred in this case. Fig. 6 shows the FTCS method mesh results in 3D.

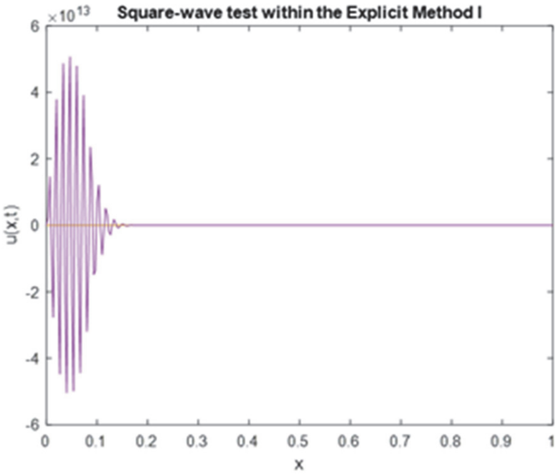

Figure 5: Square-wave (FTCS) method results for CFL=1.0

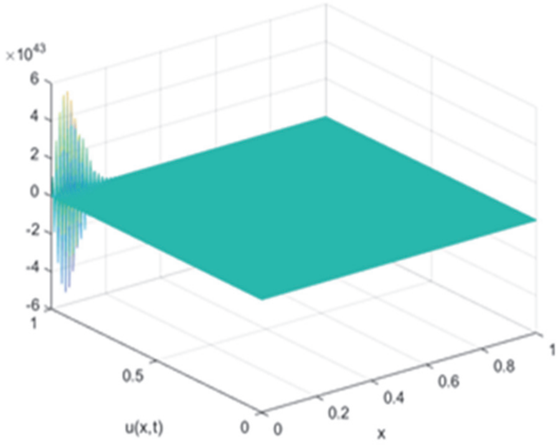

Figure 6: Square-wave (FTCS) method mesh results for CFL=1.0

The results above and the application of the von Neumann stability analysis obtain

$$\xi\left(k\right)=1-i\frac{v\Delta t}{\Delta x}\sin k\Delta x \tag{19}$$

$$CFL=\frac{c\Delta t}{\Delta x} \tag{20}$$

Thus,

$$\left|\xi\left(k\right)\right|>1 \tag{21}$$

Therefore, the solution explodes (oscillatory) and becomes unstable for Δt and Δx. The above results show that all CFL values smaller than 0.01 become the diffuser of the exact solution. For values greater than 0.01, the solution becomes unstable, as shown in the figures when CFL=1.0.

Results of Lax differencing (step-wave) method

1) CFL=0.5

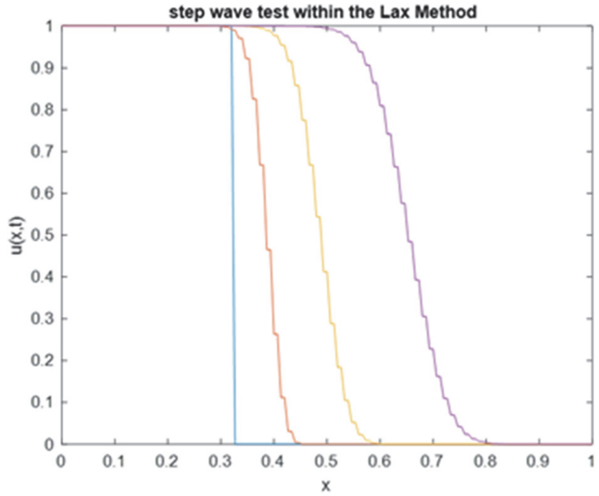

Figure 7: Lax differencing (step-wave) method results for CFL=0.5.

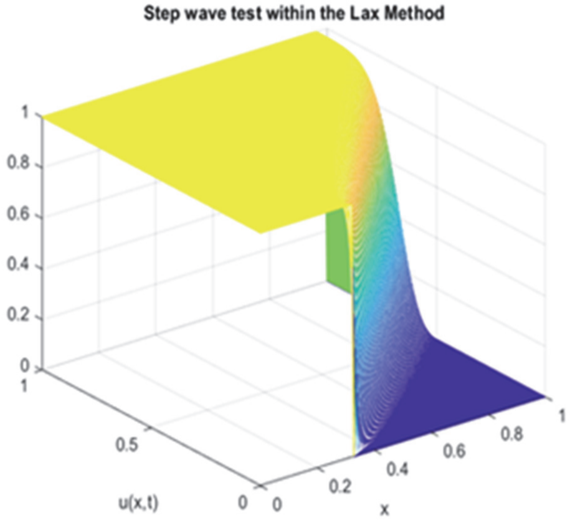

Figure 8: Lax differencing (step-wave) method mesh results for CFL=0.5

2) CFL=1.0

Fig. 9 shows the results of the Lax differencing (step-wave) method for solving the problem in the CFL=1.0 and reaching the exact solution whilst noting the value of the time taken to reach this result. Fig. 10 shows the 3D result, considering the times.

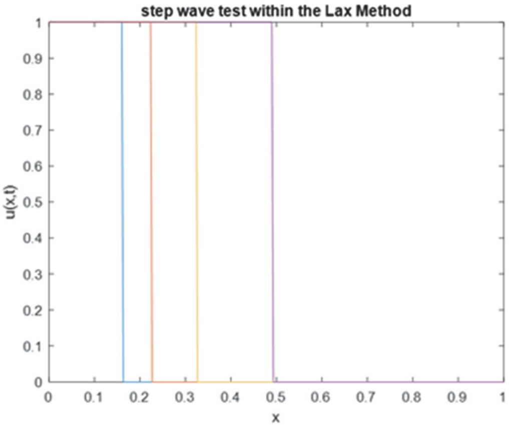

Figure 9: Lax differencing (step-wave) method result for CFL=1.0

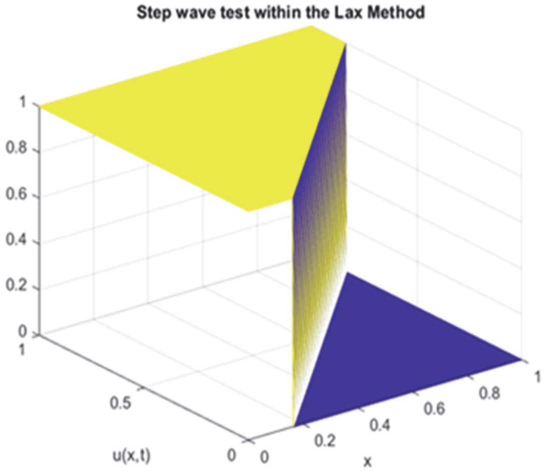

Figure 10: Lax differencing (step-wave) method mesh results for CFL=1.0

3) CFL=2.0

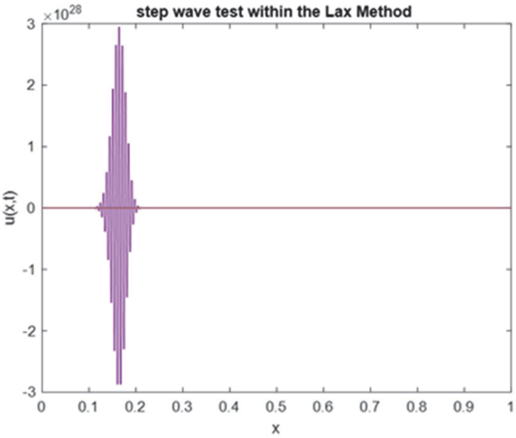

Figure 11: Lax differencing (step-wave) method results for CFL=2.0

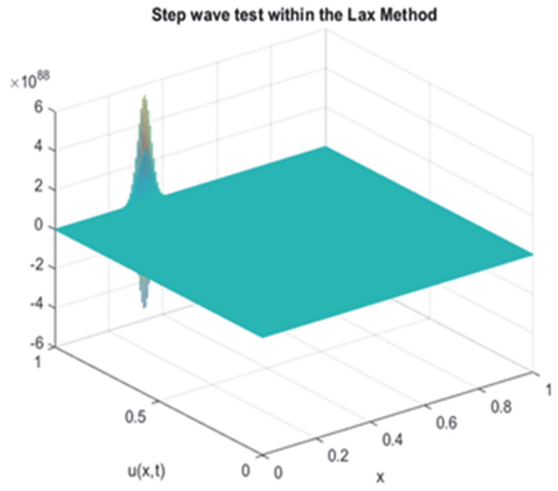

Figure 12: Lax differencing (step-wave) method mesh results for CFL=2.0

The results above and the application of the von Neumann stability analysis obtain

$$\xi = \cos k\Delta x - i\frac{c\Delta t}{\Delta x}\sin k\Delta x$$

and stability condition |ξ(k)| < 1 leads to the requirement: $CFL = c\Delta t\Delta x \leq 1$. The Lax differencing (step-wave) method must run faster than the square-wave (FTCS) method. The above results show that all CFL values smaller than 1 become the diffuser solution of the exact solution. For values greater than 1, the solution becomes unstable. This behaviour is shown in the figures when the solution reaches CFL of 2. This method can be summarised as follows:
CFL=$c\Delta t/\Delta x$>1 → The method becomes unstable.
CFL=$c\Delta t/\Delta x$<1→ The method becomes diffusive (obtaining smaller time steps worsens).
CFL=$c\Delta t/\Delta x$=1→The method converges to the exact result.

Results of One-Step Active Symmetrised Implicit Midpoint Rule

1) CFL=1.0

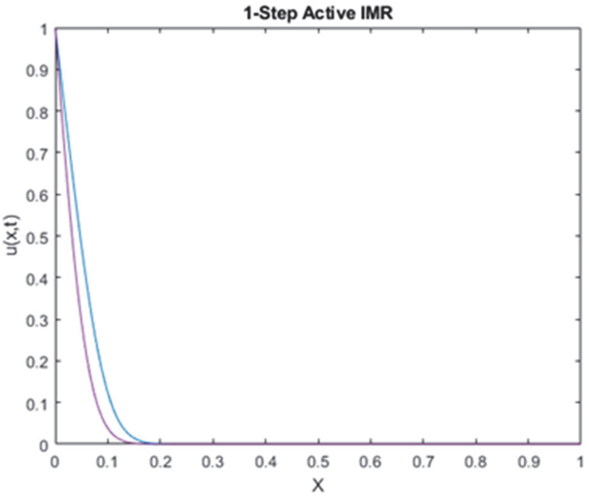

Figure 13: One-step active symmetrised IMR method results for CFL=1.0

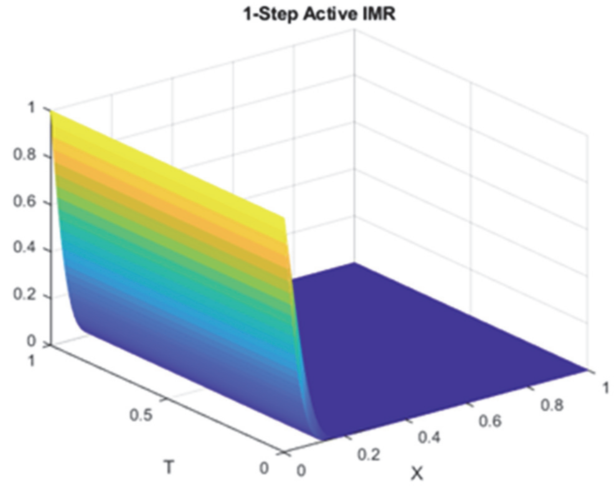

Figure 14: One-step active symmetrised IMR method mesh results for CFL=1.0

2) CFL=2.0

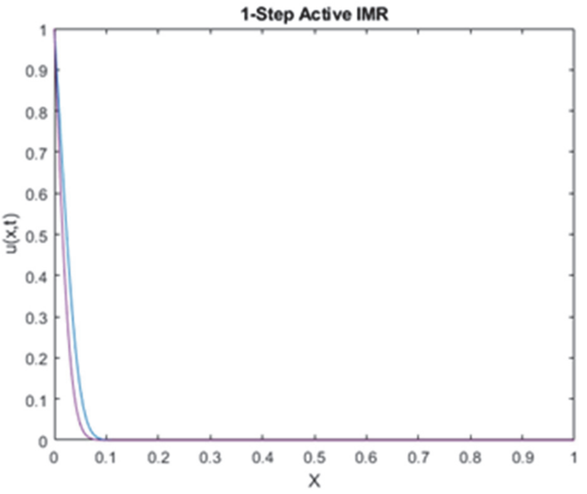

Figure 15: One-step active symmetrised IMR method results for CFL=2.0

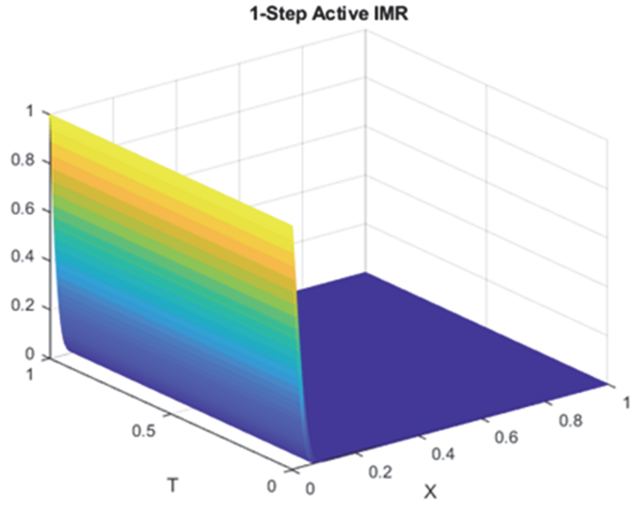

Figure 16: One-step active symmetrised IMR method mesh results for CFL=2.0

3) CFL=10.0

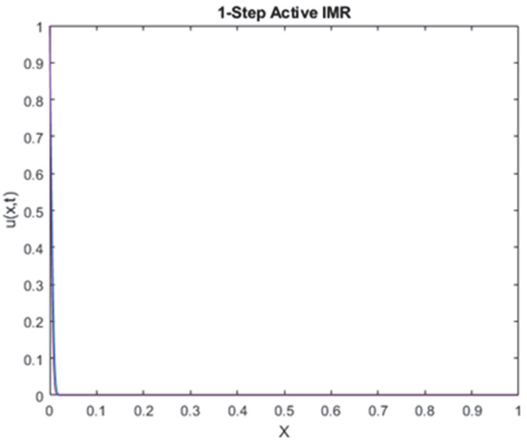

Figure 17: One-step active symmetrised IMR method results for CFL=10.0

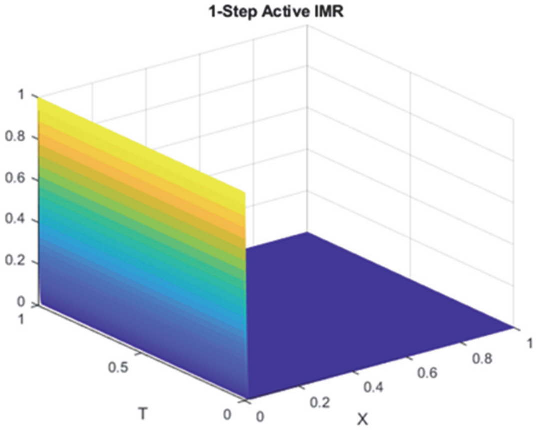

Figure 18: One-step active symmetrised IMR method mesh results for CFL=10.0

The above results and incorporating this method into an advection equation reveal that the results do not explode (oscillatory), and no convergence of the exact solution at any time is observed. The above results show that in all CFL values, the results become diffuse from the exact results, even if CFL=10.0. Although this method does not have results that focus on accurate results, it is stable for all Δt and Δx.

Results of Two-Step Active Symmetrised Implicit Midpoint Rule

1) CFL=1.0

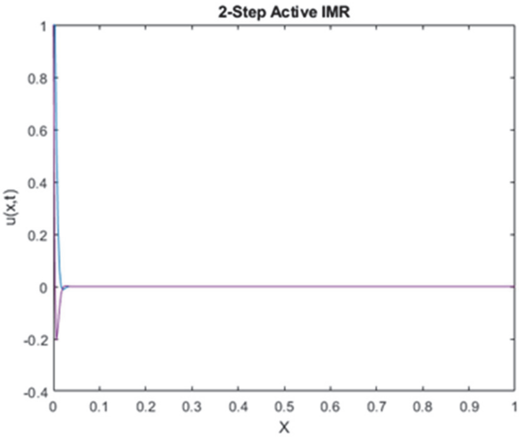

Figure 19: Two-step active symmetrised IMR method results for CFL=1.0

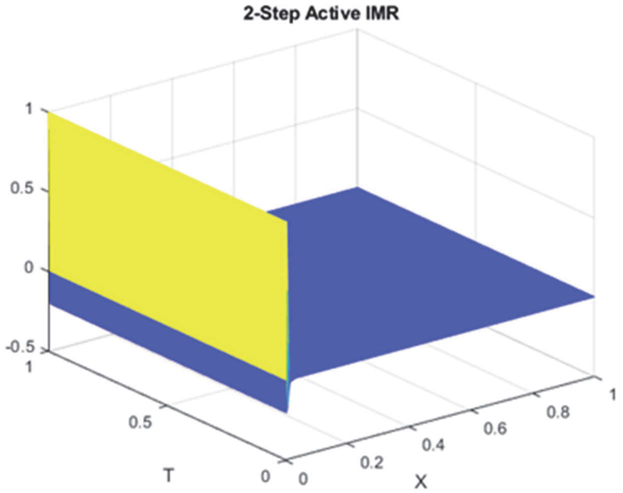

Figure 20: Two-step active symmetrised IMR method mesh results for CFL=1.0

2) CFL=2.0

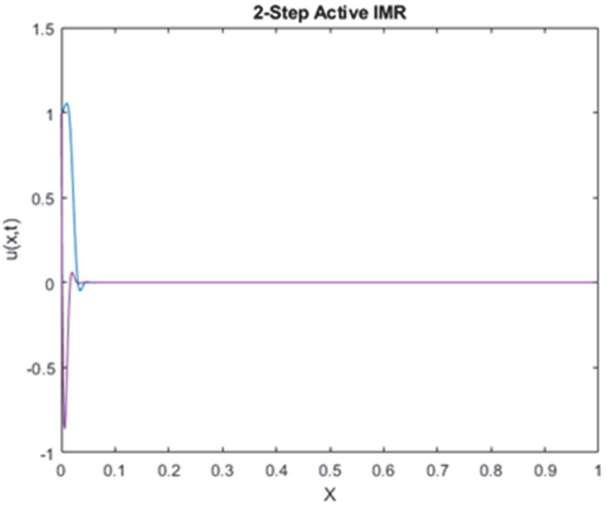

Figure 21: Two-step active symmetrised IMR method results for CFL=2.0

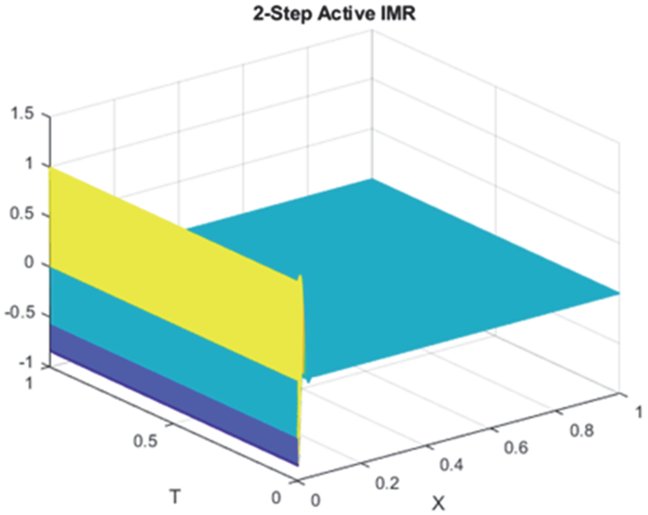

Figure 22: Two-step active symmetrised IMR method mesh results for CFL=2.0

3) CFL=10.0

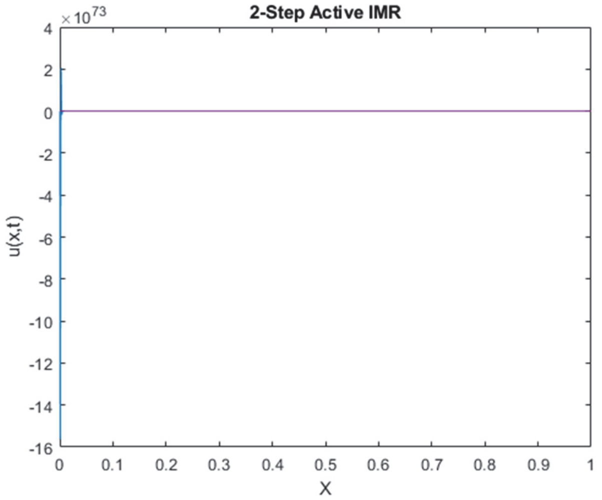

Figure 23: Two-step active symmetrised IMR method results for CFL=10.0

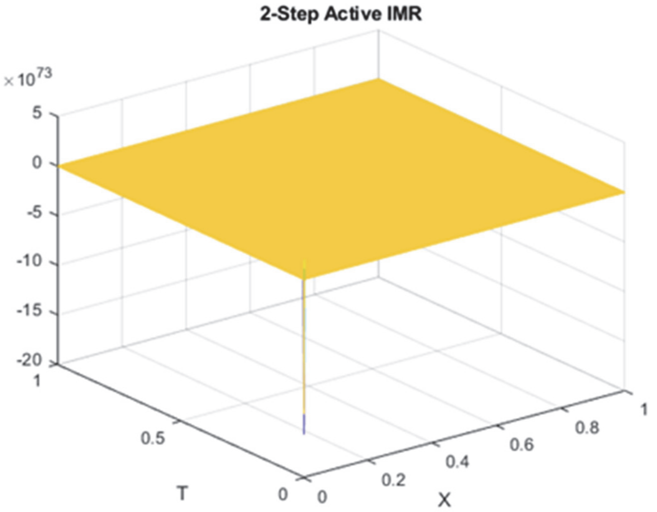

Figure 24: Two-step active symmetrised IMR method mesh results for CFL=10.0

The above results and incorporating this two-step active IMR method into the problem of an advection equation reveal that the results do not explode (oscillatory), as shown in Figs. 19–24. No convergence of the exact solution at any time is observed. The results of all CFL values become diffuse from the exact results, even if CFL=10.0. Although this method does not focus on accurate results, it is stable for all Δt and Δx.

Fig. 25 shows the solutions calculated by each method at different u and CFL=1. It shows the damping and dissipative behaviour of 1 active IMR, 2 active IMR and Lax methods as compared to the FTCS. It shows the oscillatory behaviour of the FTCS as the amplitude increases. In summary, for the square-wave (FTCS) method, the solution explodes (oscillatory) and becomes unstable for a CFL value greater than 0.01. For the step-wave Lax method, when CFL>1→ the solution is unstable, when CFL<1→the solution diffuses (obtaining smaller time steps worsens) and when CFL=1→, the solution converges to the exact solution, for the one-step active symmetrised IMR. The results do not explode (oscillate). The results of all CFL values become diffuse from the accurate results, even if CFL=10.0. Although this method does not focus on accurate results, it is stable for all Δt and Δx, for the two-step active symmetrised IMR. The results do not explode (oscillate). No convergence of the exact solution for CFL values is observed, even if CFL=10.0. Although this method does not focus on accurate results, it is stable for all Δt and Δx.

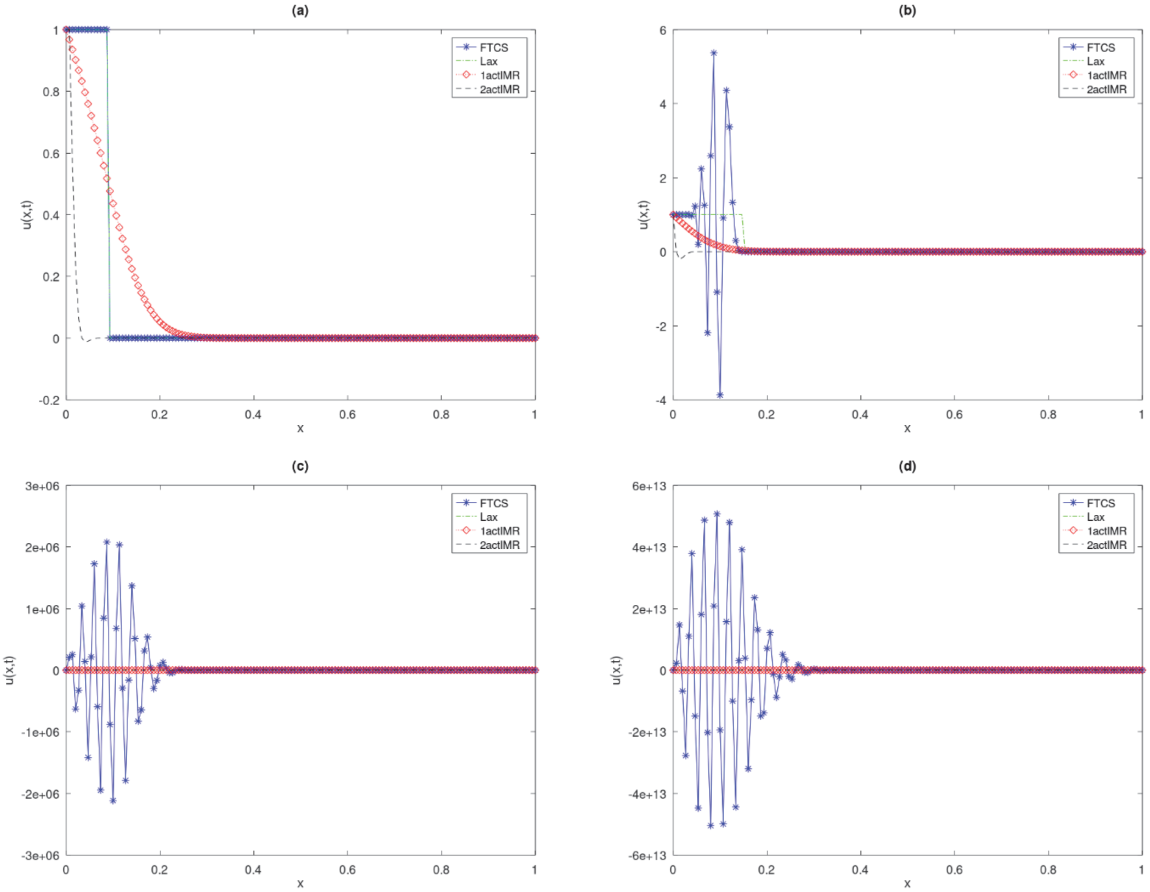

Figure 25: Solutions curve for each method at (a) $u(x,t)=1$, (b) $u(x,t)=10$, (c) $u(x,t)=50$ and (d) $u(x,t)=100$ respectively for CFL=1.0.

CONCLUSIONS

The purpose of this paper is to programme the numerical method in time and space, namely, the method of the one- and two-step active symmetrised IMR, which are suitable for CAA. No difficult calculation is needed to incorporate these two methods into the problem of the advection equation in time and space. The results of conventional methods (square-wave method [FTCS], step-wave Lax method) and FTCS method are usually unstable for hyperbolic problems, and usually unusable. Unfortunately, this FTCS equation is very limited in its use. It is an unstable method, which can only be used to study waves for low fractions for a period of oscillation. Numerical viscosity controls irregular instability and shock information, as mentioned in respect to the Lax method equation. Moreover, numerical viscosity itself is inadequate or cannot be adequately controlled. Both symmetrised IMR method methods, the one- and two-step active symmetrised IMR, are more efficient than the square-wave method (FTCS) and the step-wave Lax method. In general, this symmetrised IMR method is a numerical method used to address the problems of differential equations. The method is actively carried out at each step, in time and space, to address the problem of differential equations. The results show that both IMR methods, one- and two-step active symmetrised IMR, are stable in space and time, Δt and Δx, respectively. However, this method does not show results that reach the exact results but achieves the objective of the study, being more efficient because it is more stable in time and space compared with the two methods that are already used to solve advection equation problems, namely, the square-wave method (FTCS) and step-wave Lax method. If needed in future study, the scheme can be made even more conservative and engaging by applying the method on the different applications such as fatigue crack growth and it is of interest to contextualizing the theoretical method to a case study of a real-world problem.

ACKNOWLEDGMENTS

The authors fully acknowledge the University Kebangsaan Malaysia and the Ministry of Higher Education under Grant FRGS/1/2020/TK0/UKM/02/29 for the opportunity that made this important research viable and effective.

REFERENCES

[1] Baydoun, S. K. and Marburg, S. (2018). Quantification of numerical damping in the acoustic boundary element method for two-dimensional duct problems, Journal of Theoretical and Computational Acoustics, 26(03), 1850022.

[2] Bogey, C. and Bailly, C. (2004). A family of low dispersive and low dissipative explicit schemes for flow and noise computations. Journal of Computational Physics, 194(1), pp. 194–214. DOI: 10.1016/j.jcp.2003.09.003.

[3] Butusov, D. (2021). Adaptive stepsize control for extrapolation semi-implicit multistep ODE solvers, Mathematics, 9(9), pp. 950.

[4] Colonius, T. and Lele, S. K. (2004). Computational aeroacoustics: Progress in nonlinear problems of sound generation, Progress in Aerospace Sciences, 40(6).

[5] Chan, R. P. K. and Gorgey, A. (2013). Active and passive symmetrization of Runge-Kutta gauss methods. Applied Numerical Mathematics, 67(0), pp. 64 – 77.

[6] Citarella, R., Federico, L. and Cicatiello, A. (2007). Modal acoustic transfer vector approach in a FEM–BEM vibro-acoustic analysis, Engineering Analysis with Boundary Elements, 31(3), pp. 248-258.

[7] Farago, I., Havasi, A., Ztalev, Z. (2013). The convergence of diagonally implicit Runge-Kutta methods combined with richardson extrapolation. Comput. Math. Appl, 65(3), pp. 395-401.

[8] Ghawadri, N., Senu, N., Fawzi, F., Ismail, F. and Ibrahim, Z. (2019). Explicit integrator of Runge-Kutta type for direct solution of u(4)=f(x,u,u',u''). Symmetry, 11(2), pp. 246. DOI: org/10.3390/sym11020246.

[9] Havasi, A. and Kazemi, E. (2018). On Richardson extrapolation for low-dissipation low-dispersion diagonally implicit Runge–Kutta schemes. Journal of Computational Physics, 358, pp. 21-35.

[10] Khajah, T., Antoine, X. and Bordas, S. (2019). B-spline FEM for time-harmonic acoustic scattering and propagation. Journal of Theoretical and Computational Acoustics, 27(03).

[11] Lee, K. C., Senu, N., Ahmadian, A. and Ibrahim, S. N. I. (2020). On two-derivative Runge–Kutta type methods for solving u''' = f(x,u(x)) with application to thin film flow problem. Symmetry, 12(6), 924.
DOI: org/10.3390/sym12060924.

[12] Marburg, S. (2018). A pollution effect in the boundary element method for acoustic problems. Journal of Theoretical and Computational Acoustics, 26(02), 1850018.

[13] Marburg, S. (2017). III. A pollution effect for BEM in acoustics on Boundary Integral Methods (UKBIM 11), 3.

[14] Marburg, S. (2016). Numerical damping in the acoustic boundary element method. Acta Acustica United with Acustica, 102(3), pp. 415-418.

[15] Marburg, S. (2016). The Burton and Miller method: Unlocking another mystery of its coupling parameter. Journal of Computational Acoustics, 24(01), 1550016.

[16] Njafi-Yazdi, A. and Mongeau, L. (2013). A low-dispersion and low-dissipation implicit Runge-Kutta schemes. J. Comput. Physics, 233, pp. 315-323.

[17] Worou, C. N., Kang, J., Shen, J., Yan, P., Wang, W., Gong, Y. and Chen, Z. (2021). Runge–kutta numerical method followed by Richardson's extrapolation for efficient ion rejection reassessment of a novel defect-free synthesized nanofiltration membrane, Membranes, 11(2), pp. 130.

[18] Yao, L., Li, Y. and Li, L. (2016). Dispersion error reduction for acoustic problems using the smoothed finite element method (SFEM). International Journal for Numerical Methods in Fluids, 80(6), pp. 343-357.

[19] Xu, J., Wang, D., Huang, H., Duan, M., Gu, J. and An, C. (2017). A vortex-induced vibration model for the fatigue analysis of a marine drilling riser, Ships and Offshore Structures, 12(sup1), S280–S287.
DOI:10.1080/17445302.2016.1271557.

[20] Amann, C. and Kadau, K. (2016). Numerically efficient modified Runge–Kutta solver for fatigue crack growth analysis. Engineering Fracture Mechanics, 161, pp. 55–62. DOI: 10.1016/j.engfracmech.2016.03.